Plasmon instability in energy transfer from a current of charged particles to multiwall and cylindrical nanotube arrays based on self-consistent field theory

Antonios Balassis* and Godfrey Gumbs†
Department of Physics and Astronomy, Hunter College at the City University of New York, 695 Park Avenue, New York, New York 10021, USA
(Received 2 May 2006; published 20 July 2006)

We present a formalism for the rate of transfer of energy from a current of charged particles to multiwall and a linear array of nanotubes. The method is based on a self-consistent field theory involving Laplace's equation for the total screened potential and the density fluctuations on the nanotubes. It is demonstrated that one can identify the plasmon excitations from the spectrum of energy transfer. For a group of the excited plasmons, there is an instability associated with their decay. This occurrence is determined by the relationship between the phase velocity of the plasmon and the drift velocity of the current. A "dip" in the energy transfer spectrum corresponds to a plasmon mode instability. This is confirmed by solving the plasma dispersion equation in the complex frequency plane.

DOI: 10.1103/PhysRevB.74.045420 PACS number(s): 68.49.Uv, 34.50.Bw, 34.50.Dy

I. INTRODUCTION

Electron energy loss spectroscopy (EELS) has been used as a spectroscopic tool to probe condensed matter for many years now.[1–9] The pioneering work of Ritchie[1] on the energy loss of charged particles to a solid-state plasma slab has served as a beacon for the development of formal treatments of EELS applied to specific structures. From a theoretical point of view, the crucial quantity of interest is the nonlocal dynamic dielectric response function for the system under investigation since this quantity determines the screening properties. Experiments have been instrumental in helping us understand many phenomena. These include channeling effects observed in energy-loss spectra of nitrogen ions scattered off a Pt surface as well as charge exchange and energy dissipation of particles interacting with metal surfaces. Energy loss of helium ions in zinc has also been explored and the effective charge and the mean charge of swift ions in solids have been reported.

Recently, some attention has been given to electron energy-loss spectroscopy measurements on single-wall and multishell carbon nanotubes and their bundles.[10–16] Some of these experiments were performed using a scanning transmission-electron microscope to obtain spectra over a range of impact parameters, from the centers of the samples to several nanometers outside the material. This experimental technique provides a method for identifying the contributions from the different excitation modes. We demonstrated the contributions from single-particle and plasmon excitations for single-wall nanotubes in a recent paper.[17] Several papers have also investigated charged particle energy loss to nanotubes using various techniques and examining different aspects of the physics involved.[18–30] Here, we specifically consider the energy transfer for multishell and an array of nanotubes by developing a dielectric function formalism. Our approach allows us to identify unambiguously the contributions from the single-particle and plasmon excitations, as we did in Ref. 17, and it also shows that one of the two most energetic plasmon branches can become unstable when its phase velocity matches the drift velocity of the current used to excite them.[27] Since this plasmon instability does not arise for a single-wall nanotube, we must formulate the theory in a more general way.

The interaction of charged particles with an electron liquid confined to each tubule is described on the basis of an inverse dielectric function formalism. The simple continuum model we use can be extended to more realistic descriptions of the band structure and its related dielectric properties of experimental interest. However, the features we demonstrate are not model dependent. We use this model primarily to simplify the algebra which is still a challenge here. The response of the medium is first described in terms of the total screened potential which is self-consistently determined from the induced density from Poisson's equation. The screening is simply expressed in terms of the frequency and wave-vector-dependent longitudinal response functions for each tubule, representing the polarization cloud which follows in the wake potential of the moving charges. The electron gas is described in the random-phase approximation (RPA) of Bohm and Pines in which each momentum transfer between electrons is treated independently. This enables us to calculate the principal effects on the moving particles, including the force they experience and the resulting stopping power of the nanotubes. We describe in detail the dispersion relation of the single-particle excitations and the plasmon modes as well as the way in which they arise in the energy-transfer formula.

The formulation of the problem is first established for multishell tubules in Sec. II. Here, the axial symmetry makes it possible to employ Fourier transform techniques. In Sec. III, we extend our results to deal with a pair of nanotubes but this can be generalized to include more than two nanotubes with a more mathematically complex description. Numerical calculations are presented in Sec. IV. Here, we present the main results of our paper in which we show that for a pair of nanotubes, either coaxial or parallel, the energy transfer spectrum has a "dip" for a group of modes. We verify that these plasmon modes are unstable by solving the dispersion equation in the complex frequency plane. We add some concluding remarks in Sec. V.

II. ENERGY LOSS FOR MULTIWALL NANOTUBES

We formulate a theory for the energy-transfer for a charged particle moving parallel to the axis of a multiwall nanotube consisting of N coaxial tubules. The tubules are of radius $R_1, R_2, \ldots, R_N$ and their common axis lies along the z axis. The velocity of a moving charged particle is $\mathbf{v}=v\hat{z}$ and its position vector is $\mathbf{r}_0=(\rho_0, \phi_0, z_0=vt)$.

The total electrostatic potential and the induced charge density at any space-time point $1=(\mathbf{r}_1, t_1)$ are given, respectively, by (in this paper, we use Gaussian units)

$$V(1) = \int d^4 2 \varepsilon^{-1}(1,2) U(2), \tag{1}$$

$$\delta\rho(1) = -\frac{\varepsilon_b}{4\pi e}\nabla_1^2 \left[V(1) - \frac{1}{\varepsilon_b} U(1) \right], \tag{2}$$

where $\varepsilon^{-1}(1,2)$ is the inverse dielectric function and ε_b is the background dielectric constant of the medium where the nanotube is embedded. In this notation, we have $U(\mathbf{r},t) = Ze/|\mathbf{r}-\mathbf{r}_0(t)|$ as the potential produced by the moving charged particle which is given in cylindrical coordinates by

$$\frac{Ze}{|\mathbf{r}-\mathbf{r}_0(t)|} = \frac{Ze}{\pi} \sum_{L=-\infty}^{\infty} e^{iL(\phi-\phi_0)} \int_{-\infty}^{\infty} dq_z \times e^{iq_z(z-vt)} I_L(q_z\rho_<) K_L(q_z\rho_>), \tag{3}$$

where $\rho_<(\rho_>)$ is the smaller(larger) of ρ and ρ_0.[31] Also, $I_L(x)$ and $K_L(x)$ are modified Bessel functions. According to Eq. (3), we can write the potential $U(2)$ as (for the shake of convenience, we chose $\phi_0=0$)

$$U(2) = \frac{Z}{e} \int_{-\infty}^{\infty} \frac{dq_z}{2\pi} e^{iq_z(z_2-vt_2)} \frac{1}{2\pi} \sum_{L=-\infty}^{\infty} e^{iL\phi_2} u_L(\rho_0, \rho_2, q_z), \tag{4}$$

where $u_L(\rho_1, \rho_2, q_z)$, defined by

$$u_L(\rho_1, \rho_2, q_z) = 4\pi e^2 I_L(q_z\rho_<) K_L(q_z\rho_>), \tag{5}$$

is the Fourier transform of e^2/r for the Coulomb interaction energy in cylindrical coordinates.[31]

We use a Fourier transformation of Eq. (1) with respect to the z, ϕ, and t variables to obtain

$$V(1) = \int_0^{\infty} d\rho_2 \rho_2 \int_{-\infty}^{\infty} \frac{dq_z}{2\pi} \int_{-\infty}^{\infty} \frac{d\omega}{2\pi} e^{i(q_z z_1 - \omega t_1)} \times \frac{1}{2\pi} \sum_L e^{iL\phi_1} \varepsilon_L^{-1}(\rho_1, \rho_2, q_z, \omega) U_L(\rho_2, q_z, \omega). \tag{6}$$

From Eq. (4) we obtain

$$U_L(\rho_2, q_z, \omega) = \frac{2\pi Z}{e} u_L(\rho_0, \rho_2, q_z) \delta(\omega - v q_z) \tag{7}$$

and Eq. (6) becomes

$$V(1) = \frac{Z}{e} \int_0^{\infty} d\rho_2 \rho_2 \int_{-\infty}^{\infty} \frac{dq_z}{2\pi} e^{iq_z(z_1-vt_1)} \frac{1}{2\pi} \sum_L e^{iL\phi_1} \times u_L(\rho_0, \rho_2, q_z) \varepsilon_L^{-1}(\rho_1, \rho_2, q_z, \omega = v q_z). \tag{8}$$

Here, the inverse dielectric function $\varepsilon_L^{-1}(\rho_1, \rho_2, q_z, \omega)$ is given in the RPA by

$$\varepsilon_L^{-1}(\rho_1, \rho_2, q_z, \omega) = \frac{1}{\varepsilon_b} \frac{\delta(\rho_1-\rho_2)}{\rho_1} - \frac{1}{(2\pi)^2 \varepsilon_b^2} \sum_{j,j'=1}^{N} \frac{\delta(\rho_2 - R_{j'})}{\rho_2} \times \chi_{j,L}(q_z, \omega) u_L(\rho_1, R_j, q_z) [\mathbf{A}_L(q_z, \omega)^{-1}]_{jj'}. \tag{9}$$

The dispersion equation for plasma excitations can be determined by solving for the poles of $\varepsilon_L^{-1}(\rho_1, \rho_2, q_z, \omega)$. These poles are solutions of $\mathrm{Det}\, \mathbf{A}_L(q_z, \omega)=0$ where the matrix elements of $\mathbf{A}_L$ are

$$[\mathbf{A}_L(q_z, \omega)]_{jj'} = \delta_{jj'} + \frac{1}{(2\pi)^2 \varepsilon_b} u_L(R_j, R_{j'}, q_z) \chi_{j',L}(q_z, \omega). \tag{10}$$

Also, the polarization function of the electron gas on the jth tubule is

$$\chi_{j,L}(q_z, \omega) = 2 \sum_{l=-\infty}^{\infty} \int_{-\infty}^{\infty} dk_z \frac{f_0(\epsilon_{j,k_z,l}) - f_0(\epsilon_{j,k_z-q_z,l-L})}{\hbar\omega - (\epsilon_{j,k_z,l} - \epsilon_{j,k_z-q_z,l-L}) + i0^+}, \tag{11}$$

where $f_0(\epsilon)$ is the Fermi-Dirac distribution function and $\epsilon_{j,k_z,l} = \frac{\hbar^2 k_z^2}{2m^*} + \frac{\hbar^2 l^2}{2m^* R_j^2}$ is an energy eigenvalue on the jth tubule for an electron with effective mass m^* and $k_z, l = 0, \pm 1, \pm 2, \ldots$, are the linear and angular momentum quantum numbers of an eigenstate.

Substituting Eqs. (4) and (8) into Eq. (2), we obtain an expression for the induced charge density $\delta\rho(1)$ at any space-time point which is given by

$$\delta\rho(1) = -\frac{Z\varepsilon_b}{4\pi e^2} \int_{-\infty}^{\infty} \frac{dq_z}{2\pi} e^{iq_z(z_1-vt_1)} \frac{1}{2\pi} \sum_{L=-\infty}^{\infty} e^{iL\phi_1} \times \left\{ \int_0^{\infty} d\rho_2 \rho_2 u_L(\rho_0, \rho_2, q_z) \left[-q_z^2 - \frac{L^2}{\rho_1^2} + \frac{1}{\rho_1} \frac{\partial}{\partial \rho_1} \left(\rho_1 \frac{\partial}{\partial \rho_1} \right) \right] \varepsilon_L^{-1}(\rho_1, \rho_2, q_z, \omega = q_z v) + \frac{4\pi e^2}{\varepsilon_b} \frac{\delta(\rho_1-\rho_0)}{\rho_1} \right\}. \tag{12}$$

However, the force on the charged particle and its rate of loss of energy are given by

$$\mathbf{F} = e \int d^3 1 \, \delta\rho(1) \nabla_1 V(1) \text{ and } \frac{dW}{dt} = \mathbf{F} \cdot \mathbf{v} = F_z v, \tag{13}$$

where the z component of the force is

$$F_z = i\frac{Z^2\varepsilon_b}{16\pi^3 e^2}\int_0^\infty d\rho_1\rho_1\int_0^\infty dq_z q_z \sum_{L=-\infty}^{\infty}\left\{\frac{4\pi e^2}{\varepsilon_b}\frac{\delta(\rho_1-\rho_0)}{\rho_1} - \int_0^\infty d\rho_2\rho_2 u_L(\rho_0,\rho_2,q_z)\left[q^2+\frac{L^2}{\rho_1^2} - \frac{1}{\rho_1}\frac{\partial}{\partial\rho_1}\left(\rho_1\frac{\partial}{\partial\rho_1}\right)\right]\varepsilon_L^{-1}(\rho_1,\rho_2,q_z,\omega=vq_z)\right\} \times \int_0^\infty d\rho_3\rho_3 u_L(\rho_0,\rho_3,q_z)\varepsilon_L^{-1}(\rho_1,\rho_3,-q_z,\omega=-vq_z). \tag{14}$$

The q_z integral for the second term in curly brackets on the right-hand side of Eq. (14) is identically zero because the integrand is an odd function of q_z. This can be proven if we use the following symmetry properties for the inverse dielectric function, i.e.,

$$\varepsilon_L^{-1}(\rho_1,\rho_2,q_z,\omega) = \varepsilon_L^{-1}(\rho_1,\rho_2,-q_z,\omega), \tag{15}$$

$$\mathrm{Re}[\varepsilon_L^{-1}(\rho_1,\rho_2,q_z,\omega)] = \mathrm{Re}[\varepsilon_L^{-1}(\rho_1,\rho_2,q_z,-\omega)], \tag{16}$$

$$-\mathrm{Im}[\varepsilon_L^{-1}(\rho_1,\rho_2,q_z,\omega)] = \mathrm{Im}[\varepsilon_L^{-1}(\rho_1,\rho_2,q_z,-\omega)]. \tag{17}$$

Therefore, Eq. (14) simplifies and gives the following result:

$$F_z = \frac{Z^2}{4\pi^2}\int_{-\infty}^{\infty} dq_z i q_z \sum_{L=-\infty}^{\infty}\int_0^\infty d\rho_3\rho_3 u_L(\rho_0,\rho_3,q_z) \times\varepsilon_L^{-1}(\rho_0,\rho_3,q_z,\omega=-vq_z). \tag{18}$$

Furthermore, if we express $\varepsilon_L^{-1}(\rho_0,\rho_2,q_z,\omega)$ in terms of its real and imaginary parts and use Eqs. (9) and (15), we finally obtain

$$F_z = -\frac{Z^2}{8\pi^4\varepsilon_b^2}\sum_{L=-\infty}^{\infty}\int_0^\infty dq_z q_z \sum_{j,j'=1}^{N} u_L(\rho_0,R_j,q_z)u_L(\rho_0,R_{j'},q_z) \times \mathrm{Im}\{\chi_{j,L}(q_z,\omega=vq_z)[\mathbf{A}_L^{-1}(q_z,\omega=vq_z)]_{jj'}\} \tag{19}$$

which in turn gives the rate of loss of energy as

$$\frac{dW}{dt} = -\frac{Z^2 v}{8\pi^4\varepsilon_b^2}\sum_{L=-\infty}^{\infty}\int_0^\infty dq_z q_z \sum_{j,j'=1}^{N} u_L(\rho_0,R_j,q_z)u_L(\rho_0,R_{j'},q_z) \times \mathrm{Im}\{\chi_{j,L}(q_z,\omega=vq_z)[\mathbf{A}_L(q_z,\omega=vq_z)^{-1}]_{jj'}\}, \tag{20}$$

with matrix elements $[\mathbf{A}_L(q_z,\omega)]_{jj'}$ given by Eq. (10).

We will obtain a closed form analytic expression for the rate of loss of energy explicitly in terms of the dielectric response functions for the nanotube. To do this, we express the matrix elements of the inverse matrix as

$$[\mathbf{A}_L(q_z,\omega)^{-1}]_{jj'} = \frac{C_{L,jj'}(q_z,\omega)}{\mathrm{Det}\,\mathbf{A}_L(q_z,\omega)}, \tag{21}$$

$$\mathrm{Det}\,\mathbf{A}_L(q_z,\omega) = \mathcal{D}_{1,L}(q_z,\omega) + i\mathcal{D}_{2,L}(q_z,\omega), \tag{22}$$

where $C_{L,jj'}$ are the matrix elements of an $N\times N$ matrix and $\mathcal{D}_{1,L}(q_z,\omega)$ and $\mathcal{D}_{2,L}(q_z,\omega)$ denote the real and imaginary parts of $\mathrm{Det}\,\mathbf{A}_L(q_z,\omega)$. Equation (20) can be written as

$$\frac{dW}{dt} = -\frac{2Z^2 v}{(2\pi)^4\varepsilon_b^2}\sum_{j,j'=1}^{N}\sum_{L=-\infty}^{\infty}\int_0^\infty dq_z u_L(\rho_0,R_j,q_z)u_L(\rho_0,R_{j'},q_z) \times \left\{\mathrm{Re}\left[\frac{1}{\mathrm{Det}\,\mathbf{A}_L(q_z,\omega)}\right]\mathrm{Im}[\chi_{j,L}(q_z,\omega)C_{L,jj'}(q_z,\omega)] + \mathrm{Im}\left[\frac{1}{\mathrm{Det}\,\mathbf{A}_L(q_z,\omega)}\right]\mathrm{Re}[\chi_{j,L}(q_z,\omega)C_{L,jj'}(q_z,\omega)]\right\}\Bigg|_{\omega=vq_z}. \tag{23}$$

We now turn to analyzing the contributions to dW/dt in Eq. (23) for charged particle energy transfer. This means that we must examine when the factor $\mathrm{Im}\{\chi_{j,L}(q_z,\omega=vq_z)[\mathbf{A}_L(q_z,\omega=vq_z)^{-1}]_{jj'}\}$ in the integrand is nonzero. When there is just one tubule ($N=1$), the matrix $\mathbf{A}_L(q_z,\omega)$ becomes a scalar dielectric function $\epsilon_L(q_z,\omega)$, say, and the factor in Eq. (23) is $\propto -1/\epsilon_L(q_z,\omega)=\epsilon_I/(\epsilon_R^2+\epsilon_I^2)$, where ϵ_R and ϵ_I are the real and imaginary parts of ϵ_L. Therefore, the only contributions to dW/dt arise when either ϵ_I is finite, i.e., from the single-particle excitations on the nanotube, or when *both* ϵ_R and ϵ_I vanish simultaneously. This latter contribution comes from the plasmon excitations which are not Landau damped by the particle-hole modes. These excitations contributing to the energy transfer must have a phase velocity which coincides with the charged particle speed since $\omega=vq_z$ must be satisfied in the dielectric response function. The case for a multiwall nanotube may be analyzed in a similar way. The two terms in curly brackets in the integrand of Eq. (23) contribute *separately* unlike the case of a single-wall nanotube. The plasmon dispersion relation corresponds to $\mathrm{Det}\,\mathbf{A}_L(q_z,\omega)=0$, i.e., when both its real $[\mathcal{D}_{1,L}(q_z,\omega)]$ and imaginary $[\mathcal{D}_{2,L}(q_z,\omega)]$ parts are zero. Therefore, the plasmon contribution to the charged particle energy loss comes from only the second term in Eq. (23). The single-particle excitations contribute to *both* the first and second terms when $\mathcal{D}_{2,L}(q_z,\omega)$ is finite in conjunction with either $\mathcal{D}_{1,L}(q_z,\omega)$ zero (second term only) or finite (both first and second terms). In this regard, there is no contribution when $\mathcal{D}_{1,L}(q_z,\omega)$ is finite but $\mathcal{D}_{2,L}(q_z,\omega)=0$ because the factor multiplying the $\mathcal{D}_{1,L}(q_z,\omega)$ in the numerator vanishes since the imaginary parts of the susceptibility are all zero in this case.

For clarity, we explicitly write the contribution from plasmon excitations to Eq. (23) as

$$\left.\frac{dW}{dt}\right|_{\text{plasmons}} = \frac{Z^2 v}{8\pi^3\varepsilon_b^2}\sum_{j,j'=1}^{N}\sum_{L=-\infty}^{\infty}\int_0^\infty dq_z q_z u_L(\rho_0,R_j,q_z) \times u_L(\rho_0,R_{j'},q_z)\frac{\delta(\omega-\omega_L(q_z))}{|d\mathcal{D}_{1,L}(q_z,\omega)/d\omega|_{\omega=vq_z}} \times \mathrm{Re}\,[\chi_{j,L}(q_z,\omega)C_{L,jj'}(q_z,\omega)]|_{\omega=vq_z}, \tag{24}$$

where $\omega_L(q_z)$ is the plasmon excitation frequency for fixed

angular momentum transfer L, i.e., this is the solution of the equation $\mathrm{Det}\,\mathbf{A}_L(q_z,\omega)=0$. The contributions to Eq. (23) from single-particle excitations and polarization of the medium are straightforward to obtain. For the double-wall nanotube, i.e., $N=2$, which we do numerical calculations for, the matrix $\mathbf{C}_L(q_z,\omega)$ is

$$\mathbf{C}_L(q_z,\omega)=\begin{pmatrix} \varepsilon_{2,L}(q_z,\omega) & \dfrac{-\chi_{2,L}(q_z,\omega)u_L(R_1,R_2,q_z)}{(2\pi)^2\varepsilon_b} \\ \dfrac{-\chi_{1,L}(q_z,\omega)u_L(R_1,R_2,q_z)}{(2\pi)^2\varepsilon_b} & \varepsilon_{1,L}(q_z,\omega) \end{pmatrix}, \tag{25}$$

where $\varepsilon_{j,L}(q_z,\omega)=1+\frac{1}{(2\pi)^2\varepsilon_b}u_L(R_j,R_j,q_z)\chi_{j,L}(q_z,\omega)$ is the dielectric response function for momentum transfer with quantum number L on the jth tubule. Since setting $\varepsilon_{j,L}(q_z,\omega)=0$ yields the plasmon excitations on each tubule, it means that the $j=j'$ terms in the sums in Eqs. (23) and (24) yield the contributions to the energy-loss from each individual tubule as if there is no intertubule Coulomb interaction. The $j\neq j'$ terms give the energy loss as a result of the interaction of the charged particle with the two coupled tubules. This is so because the off-diagonal elements of the matrix $\mathbf{C}_L(q_z,\omega)$ are proportional to $u_L(R_1,R_2,q_z)$ which arises from the Coulomb interaction between the two nanotubes. However, this separation cannot be made when $N>2$ since the diagonal elements of $\mathbf{C}_L(q_z,\omega)$ contain intratubule and intertubule Coulomb effects. We note that the Coulomb interaction $u_L(R_j,R_{j'},q_z)$ between tubules could be weak compared with the coupling between electrons on the same tubule. Consequently, $\mathbf{C}_L(q_z,\omega)$ is diagonal and only $\Sigma_{j=j'}$ survives in Eq. (23). In this case, the particle energy-loss is a sum of terms due to individual tubules.

III. ENERGY TRANSFER TO A LINEAR ARRAY OF NANOTUBES

The formalism presented above for the charged particle energy transfer employed the axial symmetry for coaxial tubules. For a linear array of nanotubes, whose axes are along the z direction but each axis is on and perpendicular to the x axis, this symmetry is broken. Consequently, for this geometry, the method of calculation must be modified. For simplicity, we consider in this section, two single-wall nanotubes with radii R_1 and R_2 with their axes at $x=0$ and $x=a$, where $a>R_1+R_2$. An electron confined to the surface of the jth nanotube $(j=1,2)$ is described by the single particle eigenstates and energy eigenvalues

$$\langle \mathbf{r}|j\nu\rangle=\frac{e^{ik_z z}}{\sqrt{L_z}}\Psi_{jl}[\vec{\rho}-(j-1)a\hat{x}],\quad \Psi_{jl}(\rho)=\frac{1}{\sqrt{2\pi}}e^{il\phi}\frac{1}{\sqrt{\rho}}\Phi_j(\rho), \tag{26}$$

$$\epsilon_{j\nu}=\frac{\hbar^2k_z^2}{2m^*}+\frac{\hbar^2l^2}{2m^*R_j^2}, \tag{27}$$

where $\nu=\{k_z,l\}$ labels the eigenstates of an electron, $\Phi_j^2(\rho)=\delta(\rho-R_j)$. We find that the inverse dielectric function ε^{-1} is given by the expression

$$\varepsilon^{-1}(\vec{\rho}_1,\vec{\rho}_2,q_z,\omega)=\frac{1}{\varepsilon_b}\delta(\vec{\rho}_1-\vec{\rho}_2)-\frac{e^2}{\pi\varepsilon_b}\sum_{j=1}^{2}\sum_{m,m'=-\infty}^{\infty}\chi_{j,m}(q_z,\omega)\times K_{j,m}(\vec{\rho}_2,q_z,\omega)w_{jmm'}(q_z,R_j,\rho_1,a)e^{-im'\varphi_1}, \tag{28}$$

where

$$w_{jmm'}(q_z,\rho_1,\rho_2,a)\equiv\int_0^\infty dq_\perp\frac{q_\perp}{q_\perp^2+q_z^2}J_m(q_\perp\rho_1)J_{m'}(q_\perp\rho_2)J_{m'-m}[(j-1)q_\perp a],$$

$$K_{j,m}(\vec{\rho}_2,q_z,\omega)\equiv\int d\rho_3\Psi_{jl}^*(\vec{\rho}_3)\Psi_{jl'}(\vec{\rho}_3)\times\varepsilon^{-1}[\vec{\rho}_3+(j-1)a\hat{x},\rho_2,q_z,\omega]. \tag{29}$$

The unknown quantities $K_{j,m}(\vec{\rho}_2,q_z,\omega)$ can be obtained as solution of the set of simultaneous linear equations

$$\sum_{j'=1}^{2}\sum_{m'=-\infty}^{\infty}\left[\delta_{jj'}\delta_{mm'}+\frac{e^2}{\pi\varepsilon_b}\chi_{j',m'}(q_z,\omega)w_{mm'}(q_z,R_j,R_{j'},a)\right]\times K_{j',m'}(\vec{\rho}_2,q_z,\omega)=\frac{1}{\varepsilon_b}\Psi_{jl}^*(\vec{\rho}_2-(j-1)a\hat{x})\Psi_{jl'}[\vec{\rho}_2-(j-1)a\hat{x}]. \tag{30}$$

The dispersion equation for plasmon excitations can be found solving for the poles of $\varepsilon^{-1}(\vec{\rho}_1,\vec{\rho}_2,q_z,\omega)$ which are given by the condition $\mathrm{Det}\,\mathbf{A}(q_z,\omega)=0$ where A is the matrix with elements

$$A_{jmj'm'}(q_z,\omega) = \delta_{jj'}\delta_{mm'} + \frac{e^2}{\pi\varepsilon_b}\chi_{j',m'}(q_z,\omega)U_{mm'}(q_z,R_j,R_{j'},a). \tag{31}$$

In this notation

$$U_{mm'}(q_z,R_j,R_{j'},a) = \int_0^\infty dq_\perp \frac{q_\perp}{q_\perp^2+q_z^2} J_m(q_\perp R_j)J_{m'}(q_\perp R_{j'})J_{m'-m}[(j-j')q_\perp a]. \tag{32}$$

The same dispersion equation for the plasma modes had been obtained in Refs. 27 and 32. A particle of charge Ze moving parallel to the pair of nanotubes with a position vector $\mathbf{r}_0=(\vec{\rho}_0,z_0=vt)$, where v is the speed of the particle, creates an electrostatic potential $U(\mathbf{r},t)$ at any space-time point $(\mathbf{r},t)$ which is given by Eq. (4).The total potential and the induced charge density at any space-time point 1 are given, respectively, by Eqs. (1) and (2). Also, because of the induced charge density, the force exerted on the moving charged particle is $\mathbf{F}=e\int d^3 3\,\delta\rho(1)\nabla_1 V(1)$. After some algebra, we obtain the z component of this force which is responsible for the frictional energy loss of the particle. Our calculation then gives for the rate of loss of energy as

$$\frac{dW}{dt} = F_z v = i\frac{Z^2}{(2\pi)^4\varepsilon_b} v\int_{-\infty}^{\infty} dq_z q_z \times \sum_{j=1}^{2}\sum_{m,n,m'} \chi_{j,m}(q_z,\omega)F_{j,n,m}(\vec{\rho}_0,q_z,\omega)\Bigg\{ G_{m,m'}(\vec{\rho}_0,q_z,a) - \frac{e^2}{\pi}\sum_{j'=1}^{2}\sum_{s,p}(-1)^s \chi_{j',s}(q_z,-\omega) \times F_{j',s,p}(\vec{\rho}_0,q_z,-\omega)L_{jj',mm',s}(q_z,a)\Bigg\}, \tag{33}$$

where

$$F_{j,n,m}(\vec{\rho}_0,q_z,\omega) = e^{-in\phi_0}\int d\vec{\rho}_2 e^{in\phi_2}u_n(\rho_0,\rho_2,q_z) \times K_{j,m}(\vec{\rho}_2,q_z,\omega), \quad \omega = q_z v,$$

$$G_{m,m'}(\vec{\rho}_0,q_z,a) = e^{-im'\phi_0}\int_0^\infty dq_\perp q_\perp J_m(q_\perp R_j) \times J_{m'-m}[(j-1)q_\perp a] \times \int_0^\infty d\rho_1\rho_1 J_{m'}(q_\perp\rho_1)u_{m'}(\rho_1,\rho_0,q_z),$$

$$L_{jj',mm',s}(q_z,a) = \int_0^\infty dq_\perp \frac{q_\perp}{q_\perp^2+q_z^2} J_m(q_\perp R_j)J_{m'-m}[(j-1)q_\perp a] \times J_s(q_\perp R_j')J_{m'+s}[(j'-1)q_\perp a]. \tag{34}$$

When we take the limit $a\to\infty$, Eq. (33) reduces to the result given for one nanotube.[17] We investigate the simplest case where $R_1=R_2=R$ and the angular momentum transfer $m=l-l'$ of the plasmon excitations is zero. In this case, the energy loss formula given by Eq. (33) takes the form

$$\frac{dW}{dt} = -\frac{Z^2e^2}{4\pi^4\varepsilon_b{}^2} v\int_0^\infty dq_z q_z \int_0^\infty dq_\perp \frac{q_\perp}{q_\perp^2+q_z^2} J_0(q_\perp R)J_0(q_\perp\rho_0) \times \int_0^{2\pi} d\phi \sum_{n=-\infty}^{\infty}\sum_{j,j'=1}^{2} J_0((j-1)q_\perp a) \times e^{in[f_{j'}(\phi)-\phi_0]}u_{nj'}[\rho_0,\rho_{j'}(\phi),q_z] \times \mathrm{Im}[\chi_0(q_z,\omega=vq_z)A^{-1}_{jj'}(q_z,\omega=vq_z)]. \tag{35}$$

Here, the Coulomb potential energy $u_{nj'}[\rho_0,\rho_{j'}(\phi),q_z]$ has the same form as Eq. (5). The dependence $\rho_{j'}(\phi)$ arises since the distance from the axis of the first nanotube to the surface of the second one is a function of the polar angle. The matrix $A_{jj'}(q_z,\omega)$ is given by Eq. (31) when we use $m=m'=0$ and the functions $\rho_{j'}(\phi)$ and $f_{j'}(\phi)$ are given, respectively, by the expressions

$$\rho_{j'}(\phi) = [R^2+(j'-1)^2a^2+2aR(j'-1)\cos\phi]^{1/2},$$

$$f_{j'}(\phi) = \sin^{-1}\left(\frac{R\sin\phi}{\rho_{j'}(\phi)}\right). \tag{36}$$

The separation of the last factor in Eq. (33) into the real and imaginary parts of the determinant of the matrix $\mathbf{A}$ again identifies the contributions to the energy loss.

IV. NUMERICAL RESULTS AND DISCUSSION

In this section, we present numerical results for the energy transfer and plasmon excitation spectra for a double-wall nanotube and for a pair of single-wall nanotubes whose axes are parallel. The calculations are based on the formulas we derived above in Secs. II and III. Our results are presented in Figs. 1–6. In Figs. 1(a)–1(c), we plot the plasmon contributions to dW/dt for various impact parameters for chosen R_1 and R_2 of a double-wall nanotube. Figure 2 shows the single-particle excitation contribution for the same pair of tubules in Fig. 1. There are six plasmon branches, with the highest branch at resonance with the impinging charged particle velocity when its phase velocity is $v=1.63v_F$, the second highest branch when $v=1.25v_F$ and subsequent branches as indicated on the plasmon dispersion relation in Fig. 3. In this figure, only the plasmon branches which are not Landau damped by the single-particle excitations are given in this plot. The abrupt termination of the plasmon modes in Fig. 3 arises when the plasmon branches enter the single-particle excitation regions. There are three plasmon branches for each uncoupled tubule, i.e., when the Coulomb interaction between the tubules is neglected. This is the reason why there are six plasmon branches in Fig. 3. All of the branches in Fig. 3 *either* have a corresponding peak or dip in Figs. 1(a)–1(c) (but some are too weak to be observed on this scale). Only the second highest branch has a "dip" in the

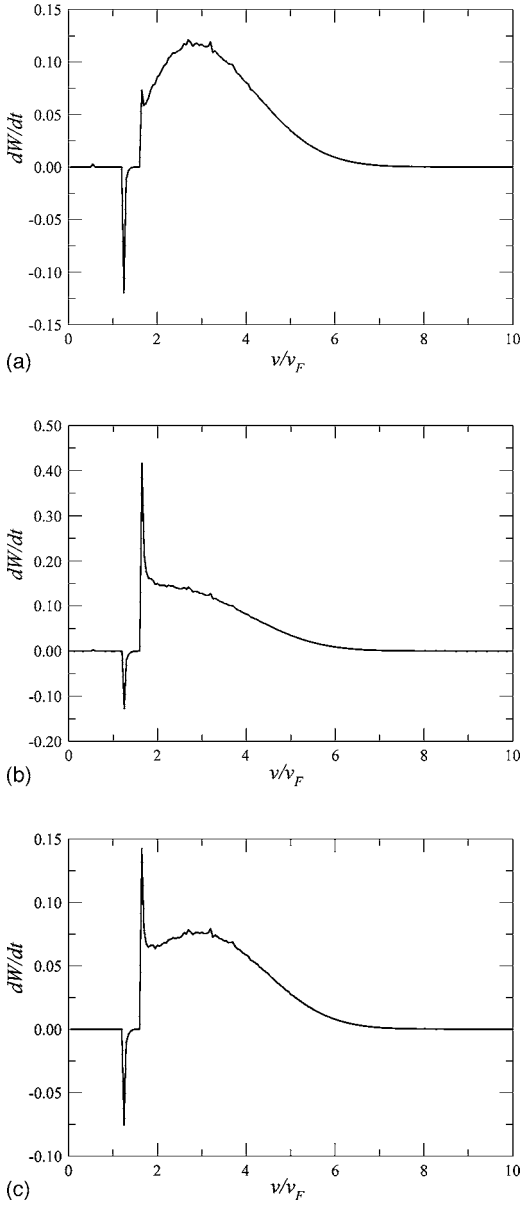

FIG. 1. The rate of energy transfer when $L=0$ due to plasmons as a function of the charged particle velocity parallel to the axis of the double-wall nanotube. The energy transfer is expressed in units of $v_F e^2 k_F^2$ and the velocity in units of v_F. In this notation, $k_F=\sqrt{2m^* E_F}/\hbar$ and $v_F=\hbar k_F/m^*$. The radii of the nanotubes are $R_1=11.0$ Å, $R_2=15.0$ Å. The Fermi energy for each nanotube is $E_F=0.6$ eV. The impact parameters for r_0 are (a) 0, (b) 10.0 Å, (c) 17.0 Å. We chose $\varepsilon_b=2.4$, the electron effective mass $m^*=0.25m_e$, where m_e is the bare electron mass.

energy transfer spectrum. We were able to identify the peaks and dips in the energy transfer spectrum by drawing the straight lines $\omega=vq_z$ which determine the energy loss contributions. When the slope of the straight line is increased and this line first touches a plasmon branch, the slope of this straight line corresponds to the resonance velocity in dW/dt. Furthermore, as the gradient of this straight line increases further, there is a range of values of particle velocity when the line sweeps through a plasmon branch. The height of the peak or depth of the dip depends on the impact parameter but

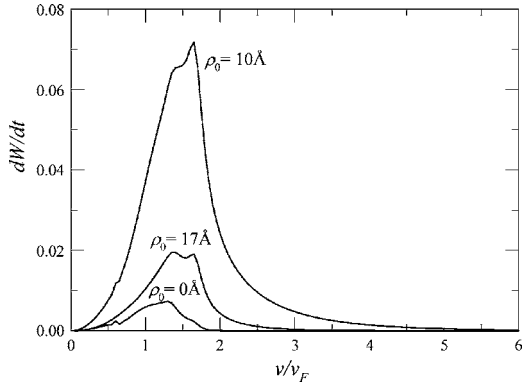

FIG. 2. The rate of loss of energy from single-particle excitations within the $L=0$ subband for a pair of coaxial tubules of radius $R_1=11.0$ Å and $R_2=15.0$ Å. All other material parameters for the background dielectric and electron effective mass are the same as Fig. 1. The values for the impact parameter ρ_0 are indicated on the plots.

its location on the velocity axis is independent of r_0. In contrast to the results in Fig. 1, Fig. 2 shows that irrespective of the impact parameter, the energy loss spectrum for single-particle excitations is always positive. The single-particle continuum corresponds to the peak positions which are also unchanged as the impact parameter is varied. However, the heights of the peaks depend on ρ_0.

We further investigate the resonance structure of Fig. 1. Except for the two most energetic plasmons, the branches of plasmon excitations lie within the gaps between single-particle excitations. In the long wavelength limit, the frequency of the second highest mode depends linearly on the wave number q_z. On the other hand, instead of having a constant phase velocity, the highest mode has a phase velocity which exhibits a logarithmic dependence on wave number.[33] Although some of the lower frequency modes have an almost constant phase velocity for small q_z, the second most energetic mode has the widest range over which the charged particle velocity could exactly coincide with its phase velocity. The dip occurs when the charged particle velocity lies in the range $1.00v_F$ to $1.50v_F$ which is shown in Fig. 3. Consequently, we must be investigate the plasmon

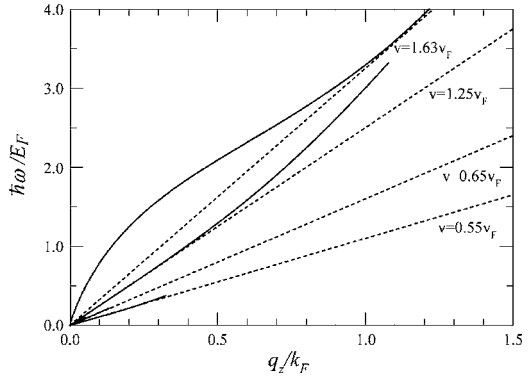

FIG. 3. The $L=0$ plasmon dispersion for the pair of coaxial nanotubes in Fig. 1. The straight lines $\omega=vq_z$ show when the plasmon branch contributes to dW/dt.

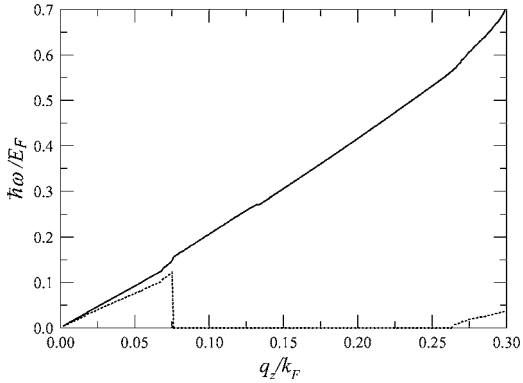

FIG. 4. The real (solid line) and imaginary (dotted line) parts of the plasmon branch with the higher frequency in the instability region in Fig. 3. The results were obtained by solving the dispersion equation in the complex frequency plane.

excitations whose frequencies lie in the region bounded by straight lines having slopes equal to these two velocities. The first step we have taken in this direction was to redo the calculation for dW/dt by excluding the plasmon branches in this region. The resulting plot showed that there was no dip. This indicates that these branches are responsible for the observed feature. The peaks in Figs. 1(a)–1(c) are similar to those we obtained for a single-wall nanotube.[17] Therefore, the physical meaning of the dip is that the plasmon branches with phase velocity in this region decay after being excited, not because they are Landau damped. Thus, the second step in our investigation was to solve the dispersion equation for complex plasmon frequencies. We obtained solutions for the frequencies whose real part lies in the bounded region $1.00v_Fq_z$ to $1.50v_Fq_z$. However, there were no such solutions outside this region. This means that the dip corresponds to a region of instability for excitations within the system and which does not include the particle-hole continuum. In Fig. 4, we plot the real and imaginary parts of the plasmon branch with the higher frequency in the instability region in Fig. 3.

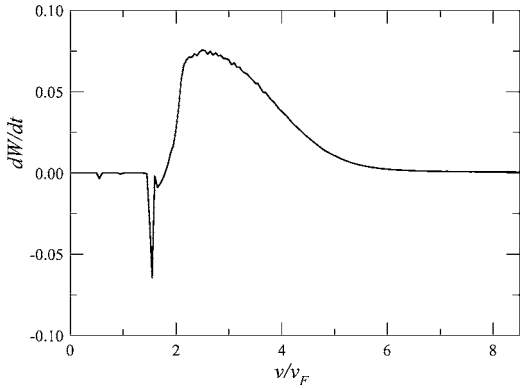

FIG. 5. The plasmon contributions to the rate of energy transfer (in units of $v_Fe^2k_F^2$) for subband transitions with $L=0$ for two parallel nanotubes each of radius $R=11.0$ Å with separation $a=25.0$ Å between them. The impact parameter of the impinging particle is $\rho_0=0$. The background dielectric constant, electron effective mass and Fermi energy for each nanotube are the same as Fig. 1.

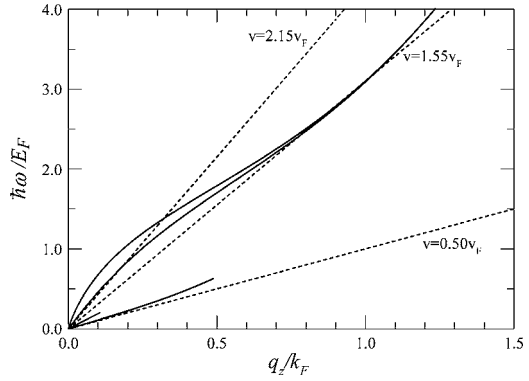

FIG. 6. The $L=0$ plasmon dispersion for the pair of parallel nanotubes in Fig. 5. The straight lines $\omega=vq_z$ show when the plasmon branch contributes to dW/dt.

These results were obtained when we solved the dispersion equation in the complex frquency plane. The real part of the plasmon frequency in Fig. 4 differs slightly from the second highest branch in Fig. 3. Also, the imaginary part of this frequency is smaller than its real part. The imaginary part increases monotonically with wave vector before rapidly decreasing around $q_z \approx 0.075\ k_F$. There is an increase in the imaginary part near $q_z \approx 0.25\ k_F$. The inverse of the imaginary part of this complex frequency yields the lifetime of the collective excitation. Thus, it is only for some ranges of wave vector where the lifetime of the plasmon excitation is "finite."

In Fig. 5, we plot the $L=0$ plasmon contribution to the rate of transfer of energy for a pair of parallel single-wall nanotubes each of radius 11.0 Å and separation $a=25.0$ Å. We chose the impact parameter as $\rho_0=0$. There are two dips in Fig. 5. These again correspond to plasmon excitations which become unstable after being excited by the charged particle. In Fig. 6, we present the plasmon excitation spectrum for the pair of parallel nanotubes used in Fig. 5. The tangent lines to the plasmon branches in Fig. 6 indicate the velocities, where the energy loss spectrum has a dip or a peak. The path of the charged particle was chosen along the axis of one of the nanotubes and the separation $a=25.0$ Å.

V. CONCLUDING REMARKS

We conclude with a discussion of plasma instabilities similar to the regions appearing in Figs. 1(a)–1(c) as well as Fig. 5. There has been considerable interest in the instabilities which arise in solid-state plasmas by the transfer of energy from a constant current to plasmon excitations generated spontaneously. This followed the pioneering work on gaseous plasmas.[34–39] Some of the solid-state plasmas include semiconductor heterostructures such as the two-dimensional electron gas (2DEG) as well as multilayered superlattices and parallel quantum wire systems. It is now known that the plasma instabilities may be driven by a direct current which flows in either the same or a neighboring layer as the plasma excitations.[36–38] As a result of the energy transfer from the current to the plasma excitations, an amplification of the collective modes may take place. This energy

could in turn be converted to electromagnetic radiation.

As in previous work, our instabilities arise when the drift velocity of the charged particles lies within a range which is determined by the phase velocity for the plasmon modes.[34,35] To show this analytically for a pair of coaxial tubules, we may use the damping theory technique, as we did for a pair of parallel nanotubes.[27] For this, one transfers to the moving frame of reference of the charged particle by replacing the momentum of an electron on the using $\hbar k_z \to \hbar k_z - m^* v$ in the response functions. In addition, we also assume that the system may still be described by the equilibrium Fermi-Dirac distribution even when a collective mode becomes unstable.

A more accurate description of the instability should employ a nonequilibrium distribution function rather than the equilibrium Fermi-Dirac function. However, this approximation is reasonable since the instability occurs in the weak nonequilibrium regime at low charged particle velocity, i.e., $v \lesssim 2v_F$. As a matter of fact, according to Echenique *et al.*[9] the low-velocity limit is defined as $v \ll v_0$, where $v_0 = e^2/\hbar = 2.19 \times 10^6$ m/s. For the parameters chosen in our calculations for Fig. 1, we have $v_0 = 2.38 v_F$. In this case, the external perturbation may be treated in linear response theory and the initial state of the electron gas on the nanotube can be treated as nearly free of scattering determined by the external probe. This approximation has been justified by Kempa *et al.*[39] in the quasiballistic limit as well as by Hu and Wilkins.[40]

ACKNOWLEDGMENTS

The authors acknowledge partial support from the National Science Foundation under Grant No. CREST 0206162 and PSC-CUNY Award No. 67172-00 36. A.B. also thanks the State Scholarship Foundation of Greece for financial support. G.G. would like to thank the Jack and Pearl Resnick Institute of Bar-Ilan University where part of this work was done for their kind hospitality. G.G. would also like to express his thanks to the U.S.-Israel Educational Foundation for additional financial support.

*Electronic address: abalassi@hunter.cuny.edu
†Electronic address: ggumbs@hunter.cuny.edu

[1] R. H. Ritchie, Phys. Rev. **106**, 874 (1957).
[2] B. N. J. Persson, Solid State Commun. **52**, 811 (1984).
[3] N. J. M. Horing, H. C. Tso, and Godfrey Gumbs, Phys. Rev. B **36**, 1588 (1987).
[4] P. M. Echenique and J. B Pendry, Prog. Surf. Sci. **32**, 111 (1989).
[5] A. Närmann, R. Monreal, P. M. Echenique, F. Flores, W. Heiland, and S. Schubert, Phys. Rev. Lett. **64**, 1601 (1990).
[6] I. Nagy, A. Arnau, and P. M. Echenique, Phys. Rev. A **40**, 987 (1989).
[7] A. Robin, W. Heiland, J. Jensen, J. I. Juaristi, and A. Arnau, Phys. Rev. A **64**, 052901 (2001).
[8] Godfrey Gumbs and N. J. M. Horing, Phys. Rev. B **43**, 2119 (1991).
[9] P. M. Echenique, F. Flores, and R. H. Ritchie, in *Solid State Physics: Advances in Research and Applications* edited by Henry Ehrenreich and David Turnbull (Academic, New York, 1990), Vol. 43, p. 230.
[10] Y. Murakami, E. Einarsson, T. Edamura, and S. Maruyama, Phys. Rev. Lett. **94**, 087402 (2005).
[11] M. Kociak, L. Henrard, O. Stephan, K. Suenaga, and C. Colliex, Phys. Rev. B **61**, 13936 (2000).
[12] B. W. Reed and M. Sarikaya, Phys. Rev. B **64**, 195404 (2001).
[13] M. Knupfer, T. Pichler, M. S. Golden, J. Fink, A. Rinzler, and R. E. Smalley, Carbon **37**, 733 (1999).
[14] F. J. Garcia-Vidal and J. M. Pitarke, Eur. Phys. J. B **22**, 257 (2001).
[15] P. M. Ajayan, S. Iijima, and T. Ichihashi, Phys. Rev. B **47**, 6859 (1993).
[16] K. Suenaga, E. Sandr, C. Colliex, C. J. Pickard, H. Kataura, and S. Iijima, Phys. Rev. B **63**, 165408 (2001).
[17] Godfrey Gumbs and Antonios Balassis, Phys. Rev. B **71**, 235410 (2005).
[18] C. W. Chiu, C. P. Chang, F. L. Shyu, R. B. Chen, and M. F. Lin, Phys. Rev. B **67**, 165421 (2003).
[19] A. Rivacoba and F. J. Garca de Abajo, Phys. Rev. B **67**, 085414 (2003).
[20] Da-Peng Zhou, You-Nian Wang, Li Wei, and Z. L. Miskovic, Phys. Rev. A **72**, 023202 (2005).
[21] N. R. Arista, Phys. Rev. A **64**, 032901 (2001).
[22] N. R. Arista and M. A. Fuentes, Phys. Rev. B **63**, 165401 (2001).
[23] N. R. Arista, Nucl. Instrum. Methods Phys. Res. B **182**, 109 (2001).
[24] D. J. Mowbray, Z. L. Miskovic, F. O. Goodman, and You-Nian Wang, Phys. Rev. B **70**, 195418 (2004).
[25] J. A. V. Pomoell, A. V. Krasheninnikov, K. Nordlund, and J. Keinonen, J. Appl. Phys. **96**, 2864 (2004).
[26] You-Nian Wang and Z. L. Miskovic, Phys. Rev. A **69**, 022901 (2004).
[27] Godfrey Gumbs and A. Balassis, Phys. Rev. B **68**, 075405 (2003).
[28] R. Vincent, J. I. Juaristi, and I. Nagy, Phys. Rev. A **71**, 062902 (2005).
[29] G. H. Lantschner, J. C. Eckardt, A. F. Lifschitz, N. R. Arista, L. L. Araujo, P. F. Duarte, J. H. R. D. Santos, M. Behar, J. F. Dias, P. L. Grande, C. C. Montanari, and J. E. Miraglia, Phys. Rev. A **69**, 062903 (2004).
[30] A. F. Lifschitz and N. R. Arista, Phys. Rev. A **69**, 012902 (2004).
[31] J. D. Jackson, *Classical Electrodynamics* (Wiley, New York, 1975).
[32] Godfrey Gumbs and G. R. Aĭzin, Phys. Rev. B **65**, 195407 (2002).
[33] Godfrey Gumbs, A. Balassis, and P. Fekete, Phys. Rev. B **73**, 075411 (2006).
[34] M. V. Krasheninnikov and A. V. Chaplik, Zh. Eksp. Teor. Fiz. **79**, 555 (1980) [Sov. Phys. JETP **52**, 279 (1980)].
[35] S. A. Mikhailov, Phys. Rev. B **58**, 1517 (1998).
[36] K. Kempa, Appl. Phys. Lett. **50**, 1185 (1987).
[37] P. Bakshi, J. Cen, and K. Kempa, J. Appl. Phys. **64**, 2243 (1988).
[38] J. Cen, K. Kempa, and P. Bakshi, Phys. Rev. B **38**, 10051 (1988).
[39] K. Kempa, P. Bakshi, J. Cen, and H. Xie, Phys. Rev. B **43**, 9273 (1991).
[40] Ben Yu-Kuang Hu and John W. Wilkins, Phys. Rev. B **43**, 14009 (1991).